PAPER

Dynamic remagnetisation of $CoFe_2O_4$ nanoparticles: thermal fluctuational thawing of anisotropy

View the article online for updates and enhancements.

Dynamic remagnetisation of CoFe$_2$O$_4$ nanoparticles: thermal fluctuational thawing of anisotropy

D A Balaev[1], I S Poperechny[2,3], A A Krasikov[1], S V Semenov[1], S I Popkov[1], Y V Knyazev[1], V L Kirillov[4], S S Yakushkin[4], O N Martyanov[4] and Yu L Raikher[2,*]

[1] Institute of Physics, Russian Academy of Sciences, Siberian Branch, Krasnoyarsk 660000, Russia

[2] Institute of Continuous Media Mechanics, Russian Academy of Sciences, Ural Branch, Perm 614068, Russia

[3] Department of Phase Transitions Physics, Perm State National Research University, Perm 614990, Russia

[4] Boreskov Institute of Catalysis, Russian Academy of Sciences, Siberian Branch, Novosibirsk 630090, Russia

E-mail: raikher@icmm.ru

Abstract
We report a study of the magnetodynamics of cobalt ferrite (CoFe$_2$O$_4$) nanoparticles with an average diameter of ~6 nm. Hysteresis loops were measured under quasi-static conditions and in pulse fields with amplitudes H$_0$ of up to 130 kOe and for durations τ_P of 8 and 16 ms. The growth of coercivity H$_c$ observed with an increase in the magnetic field variation rate dH/dt (determined by the values of H$_0$ and τ_P) and the reduction of H$_c$ with temperature is ascribed to the superparamagnetic effect. The proposed theoretical model explains the observed dependences fairly well. Notably, the effective magnetic anisotropy constant obtained exceeds the value for bulk crystals and might be indicative of the contribution of surface magnetic anisotropy.

Keywords: nanoparticles, cobalt ferrite, magnetodynamics, superparamagnetism, effective anisotropy

(Some figures may appear in colour only in the online journal)

1. Introduction

Magnetic nanoparticles have great prospects for applications in various fields of engineering and technology. Their scope comprises both classical problems (the manufacture of permanent magnets [1, 2] and catalysis [3, 4]) and the development of novel cutting-edge techniques for ecology [5–7], biotechnology [8, 9], and medicine (field-controlled drug delivery, magnetic hyperthermia, and cell surgery) [10–13].

Notwithstanding the differences between the concrete physical processes—magnetic resonance, magnetic relaxation, thermal, optical, mechanical, and other—exploited in those applications, all of them are based on the same generic effect: control over the magnetic moments of nanoparticles by means of an applied magnetic field. An attempt to optimally solve any particular task of the aforementioned kind immediately poses the question of how to choose particles of the desired quality, and this issue cannot be resolved without resorting to the fundamental material science of these objects.

Each ferromagnet or ferrite in the nanodisperse state is characterized by many parameters, whose values might be

drastically different in the bulk of a particle and on its surface. In addition, the small size of nanoparticles imparts certain peculiarities to the magnetic properties of the material, which are inessential for bulk samples. The main such properties are the superparamagnetism and exchange-bias effects. For this reason, obtaining a reliable set of parameters for a given type of nanoparticle, even if their material is well-studied *per se*, requires a vast amount of measurement and computation. The goal of this work is to refine the characteristics of a widely used nanodisperse material: cobalt ferrite ($CoFe_2O_4$). Its relatively low cost, and a coercivity higher than that of the majority of ferrites, make this material interesting for all the above-mentioned fields of application. Even from a fairly incomplete list of papers given in the bibliography below [1–44], see also reviews [8, 26, 40], one can infer that the properties of nano-$CoFe_2O_4$ have aroused continuous interest. However, such a flow of articles may suggest that comprehensive knowledge of the properties of this nanomaterial is still lacking.

One problem that is subject to intense investigation and discussion is the magnetic anisotropy of nano-$CoFe_2O_4$. Unlike nanodisperse magnetite or maghemite, where the presence of a surface contribution is fairly well proven [45], in $CoFe_2O_4$, the attribution of the origin of the particles' effective anisotropy to either the bulk alone or a combination of the bulk and the surface is still under discussion. The surface contribution to the anisotropy of nano-$CoFe_2O_4$ is mentioned in many studies [16, 17, 19–26, 28, 29, 32–34, 46, 47], and its presence is supported by evidence for a distinctive spin tilt at the outer border of the particles [27, 44, 48, 49]. The resolution of this issue seems to require a systematic investigation of magnetic anisotropy over a sufficiently large series of samples with varying mean particle sizes.

Meanwhile, a conventional approach is to consider the coercive force H_c of a nano-$CoFe_2O_4$ sample (a powder or a dilute solid dispersion) and to deduce the effective anisotropy constant as $K_{eff} = AH_cM_s$, where M_s is the particles' magnetisation at given temperature and A is a coefficient that depends on the symmetry type of the anisotropy ascribed to the particle, i.e., uniaxial or cubic.

In this work, we address the effect which, on the one hand, is universal whatever K_{eff}, and, on the other hand, enables one to estimate the feasible intervals of the energy densities K and K_s of the bulk and surface anisotropies, respectively. Our approach is based on the consistent use of superparamagnetic theory, i.e., taking into account the influence of the thermal fluctuational motion of the particles' magnetic moments on the equilibrium as well as on the magnetodynamic properties of nano-$CoFe_2O_4$. It follows from the above that nano-$CoFe_2O_4$, which we consider below, although a particularly good example, is not at all the only object that our model can be applied to.

All the works in which the magnetic measurements have covered a significant temperature range demonstrated a fast narrowing of the observed hysteresis loops (the reduction of coercivity H_c) with an increase in temperature [1, 15, 16, 18, 19, 22, 23, 25, 26, 29, 34, 37]. Figuratively speaking, the anisotropy thaws with temperature. Assuming a simple linear relation between H_c and the anisotropy constant of particles, the authors of those papers conclude that the effective anisotropy constant K_{eff} of nano-$CoFe_2O_4$ strongly depends on temperature but refrain from clarifying the origin of that behaviour. Meanwhile, the magnetic anisotropy of nanoparticles is of fundamental importance for estimating the coercivity of composites containing nano-$CoFe_2O_4$ in all practically interesting regimes: the quasi static mode, low-frequency dynamic hysteresis (the main mechanism of magnetic hyperthermia), and magnetic resonance in the radio-frequency and microwave ranges.

In this work, we report the results of measurements of the dynamic magnetisation of nano-$CoFe_2O_4$ in the range of 80 K–300 K obtained by an original technique that employs quasi-sinusoidal pulse fields and presents them along with static measurements for the 4.2 K–300 K range. On the basis of these data and using kinetic theory, we demonstrate that the rapid temperature drop of the coercivity is caused, mainly or entirely, by the superparamagnetism of nanoparticles. The paper is organised as follows. Section 2 describes the technique used for the synthesis of nanodisperse $CoFe_2O_4$ and outlines the magnetometric experiments. Section 3 presents the results of the characterization of the samples and the magnetic measurement data, while section 4 contains a theoretical interpretation of the results. Finally, we estimate quantitative bounds for the parameters of the bulk and surface contributions to particle anisotropy.

2. Synthesis of nanoparticles and investigation techniques

2.1. Synthesis of CoFe₂O₄ nanoparticles

$CoFe_2O_4$ nanoparticles were prepared by the method first described in [50], which makes it possible to obtain nanoparticles with an average diameter of 4 to 8 nm and a narrow size distribution. In this study, we examined a sample of nanoparticles obtained by co-deposition of Fe and Co salts in a rectified ethanol solution. The reagents used in the synthesis were $FeCl_3 \cdot 6H_2O$ with a purity of 99.6%, pure $CoCl_2 \cdot 2H_2O$, chemically pure propylene epoxide (PE) C_3H_6O, and rectified ethanol with a purity of 93.2%. To synthesize the $CoFe_2O_4$ ferrite, PE was added to the iron and cobalt chloride solution in rectified ethanol and mixed at room temperature for 45 min. The mixture obtained was then refluxed for 2 h to complete the reaction and to form ferrite nanoparticles. To fully remove the reaction products, the ferrite nanopowder obtained was washed with ethanol using magnetic decanting and dried in air at room temperature. The reagent ratio was calculated from the conditions $[Fe^{3+}] + [Co^{2+}] = 0.33$ mol l^{-1}, $[Fe^{3+}]/[Co^{2+}] = 2$, and PE/Cl $= 4.6$. A large excess of PE was necessary to completely and rapidly remove the Cl^- anions from the solution. To perform the magnetic measurements, the nano-$CoFe_2O_4$ produced was dispersed in paraffin at a concentration of 4 wt.%. Given the specific densities for $\rho_{ferrite} \approx 5.2$ and $\rho_{paraffin} \approx 0.9$ g cm^{-3}, one finds for a ferrite content $\phi \approx 0.7\%$ by volume.

J. Phys. D: Appl. Phys. **54** (2021) 275003

D A Balaev *et al*

2.2. Measurement techniques

X-ray diffraction (XRD) patterns of the investigated samples were obtained using a Bruker D8 Advance diffractometer (CuKα radiation, wavelength $\lambda = 1.5418$ Å). A high-resolution transmission electron microscopy (HRTEM) study was carried out using a JEOL JEM-2010 microscope at an accelerating voltage of 200 kV with a resolution of 1.4 Å. The elemental composition of the samples was examined by energy-dispersive x-ray spectroscopy (EDX).

The Mössbauer spectra of the nanoparticles were obtained using an MS-1104Em spectrometer (Research Institute of Physics, Southern Federal University, Russia) in the transmission geometry with a $Co^{57}(Rh)$ radioactive source in the temperature range of 4 K–300 K; the temperature was maintained by a CFSG-311-MESS cryostat (with the sample in the exchange gas) based on a closed-cycle Gifford-McMahon cryocooler (Cryotrade Engineering, LLC). The processing of the spectra measured at room temperature comprised two stages. First, the distributions of the hyperfine field probabilities $P(H_{hf})$ in the experimental spectra were calculated. Using the results obtained, possible nonequivalent magnetic states of iron in the samples were determined. Preliminary spectra were then formed, which were then fitted to the experimental spectra by changing the entire set of hyperfine parameters using the least-squares technique in the linear approximation.

The quasistatic magnetic properties of a paraffin-based sample of nano-$CoFe_2O_4$ were measured with a vibrating sample magnetometer (VSM) [51]. The temperature dependence of magnetisation $M(T)$ was measured after cooling in a zero external field (the zero-field cooling mode, ZFC) and in a nonzero field (the field cooling mode, FC). The field dependence of magnetisation $M(H)$ was measured under ZFC conditions. The field variation rate dH/dt used when measuring the quasi static hysteresis loops was ≈ 50 Oe s^{-1}. Note that throughout this paper, we express magnetisation in [emu g^{-1}] units, i.e. per unit mass of $CoFe_2O_4$.

2.3. Measuring the magnetic hysteresis loops in pulse fields

The magnetic hysteresis loops were measured with an original strong pulse-field setup (Kirensky Institute of Physics, Siberian Branch, Russian Academy of Sciences), which is based on a capacitor battery discharged through a solenoid. In such setups, the oscillatory process is conventionally stopped by a thyristor after the first half-wave, however, to obtain information about the coercivity, no less than two half-waves are required. To shape the second half-wave, the circuit setup was modified by shunting the thyristor with diodes. Figure 1 shows the typical time dependences of the solenoid field for a set of maximum fields H_0, whose value is determined by the capacitor's charge voltage and the pulse length described by the duration τ_P of a half-wave of the generated field. After a time lapse $t = 2\tau_P$, the field is zeroed by closing the thyristor. The value of τ_P was changed by adjusting the capacitor battery units to different capacitances; the measurements were performed at $\tau_P = 8$ and 16 ms. The magnetic field variation rate dH/dt at the instant of the sample's magnetisation switching
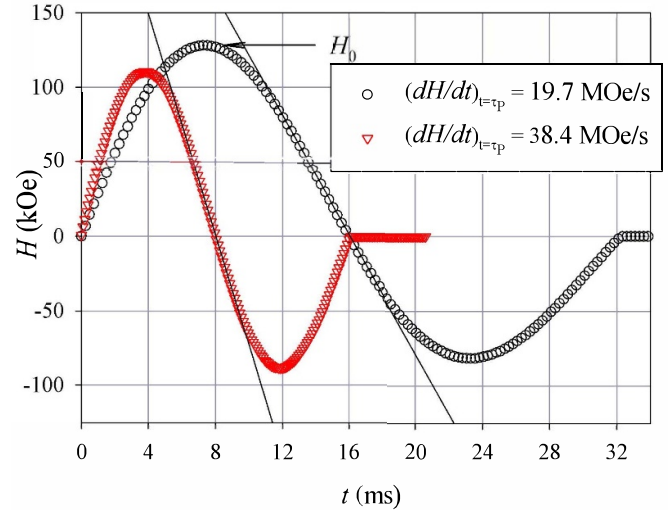

Figure 1. Typical time dependences of the solenoid field in the pulse setup for different maximum applied fields H_0; the pulse lengths τ_P are 8 and 16 ms. The slopes of the straight lines show the field variation rate dH/dt at the instant of time $t = \tau_P$, i.e., upon sample magnetisation switching.

was determined as the slope of the tangent to the $H(t)$ curve, see figure 1.

The magnetisation was measured in the temperature range of 80 K–300 K using an induction sensor consisting of a set of coaxial compensated coils located around the sample; the signal from the coils was amplified and recorded by a digital storage oscilloscope. At each temperature, a series of measurements with gradually increasing values of H_0 was undertaken.

3. Results

The XRD pattern for the sample investigated is presented in figure 2. All the observed peaks correspond to $CoFe_2O_4$ (JCPDS card 22-1086) [52]; the coherent scattering region sizes, calculated from the peak width at half-maximum using the Scherrer equations, are ≈ 6 nm.

The transmission electron microscopy data are in good agreement with the results of the XRD analysis. Figure 3(a) shows a typical HRTEM microphotograph of the sample under study. According to the EDX data (figure 3(b)), the component ratio is Fe/Co = 1.98, which is consistent with the elemental composition of cobalt ferrite. Figure 3(c) presents the particle size distribution histogram obtained by processing many microphotographs. The average particle diameter was 6 nm, which coincides with the coherent scattering region determined from the x-ray scattering data.

The Mössbauer spectrum of the investigated sample at $T = 4.2$ K is shown in figure 4(a). At this temperature, the hyperfine structure of the spectrum is not affected by superparamagnetism and demonstrates Zeeman splitting (sextet), which is indicative of blocked magnetic moments of the particles. The parameters of the spectra, including the isomer shift IS, the hyperfine field H_{hf}, and quadrupole splitting QS,
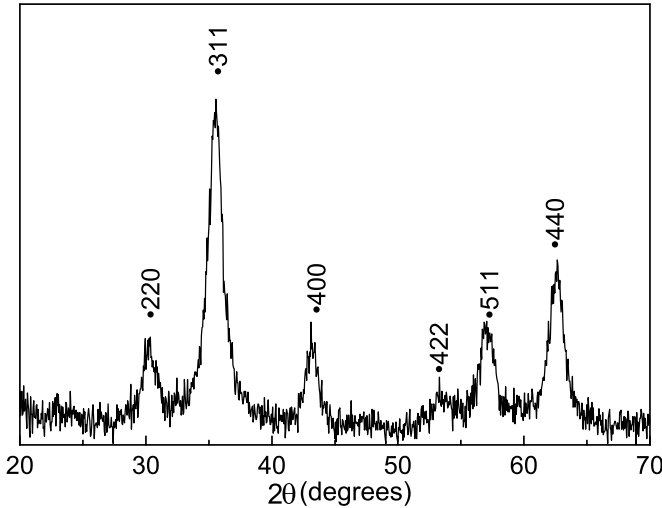
Figure 2. XRD pattern of the $CoFe_2O_4$ nanoparticle sample investigated.

given in table 1, correspond to the Mössbauer parameters of similar cobalt ferrite nanoparticles [52–54].

The hyperfine field probabilities $P(H_{hf})$ obtained reveal the existence of several magnetically nonequivalent iron sites. The broad peaks highlight a nonuniformity of the iron distribution due to the substitution of cobalt. This is evidenced by the nonzero values of the parameter dH in table 1. The isomer shift, IS, is smaller in the tetrahedral A sites of ferrite than in the octahedral B sites. This allows us to establish the distribution of Co^{2+} and Fe^{3+} cations over the ferrite crystallographic sublattices. Based on the Mössbauer data, we confirm that the crystallochemical formula for the sample is $(Co_{0.52}Fe_{0.48})[Co_{0.24}Fe_{0.76}]_2O_4$, which agrees well with the results reported in [20]. Therefore, our analysis of the Mössbauer spectra confirms once again that the synthesis performed yields cobalt ferrite nanoparticles with a component ratio of Co/Fe = 1/2.

Figure 5 shows the temperature dependences of magnetisation $M(T)$ measured using the ZFC and FC protocols under fields of $H = 1$ and 10 kOe. The pronounced maxima of the $M(T)_{ZFC}$ plots and the bifurcations of $M(T)_{ZFC}$ and $M(T)_{FC}$ curves are evidence that in the samples under study, the particles' magnetic moments become blocked when subjected to a temperature decrease, i.e., they exhibit typical superparamagnetic behaviour. The position of the $M(T)_{ZFC}$ maximum at a moderate field of 1 kOe is $\approx$290 K, which is in good agreement with the data reported by other authors for $CoFe_2O_4$ nanoparticles of similar size [55–57]. With an increase in the applied field, the maximum of the function $M(T)_{ZFC}$ shifts toward lower temperatures, as expected.

The quasistatic magnetic hysteresis loops $M(H)$ recorded by the VSM technique together with the same dependences recorded using pulsed fields are shown in figure 6. As mentioned, measurements in pulsed fields do not allow one to monitor the entire magnetic hysteresis loop. However, all its important fragments are available; specifically, one can obtain the following portions of the $M(H)$ curve: (I) from zero to H_0,

(II) from H_0 to the negative field H_0^* (note that $|H_0^*|$ is somewhat smaller than H_0), and (III) from H_0^* to zero, see figure 1.

The most informative part of the loop is portion (II), where the intersection of the $M(H)$ curve with the abscissa axis in the negative field range determines the coercivity H_c. It can be seen in figure 6 that an increase in the field variation rate dH/dt leads to a significant growth of the absolute value of H_c, which is characteristic of dynamic magnetisation switching in single-domain magnetic nanoparticles.

The field variation rates dH/dt indicated in figure 6 correspond to the pulse parameters given in table 2. By changing the maximum applied field H_0 and the pulse length τ_P (8 and 16 ms), which determine the parameter dH/dt, we have measured the $H_c(dH/dt)$ dependences at different temperatures; these results are presented in figure 7. One can see that the coercivity grows monotonically with increasing dH/dt whereas an increase in temperature reduces $|H_c|$. A theoretical analysis of this behaviour in the framework of kinetic theory is given in the next section.

4. Theoretical analysis

As can be seen from figure 6, the magnetisation loops measured in any mode narrow significantly with an increase in temperature, thus revealing the strong influence of thermal motion on the magnetic response of the dispersed nanoparticles. To account for this, one has to allow for particle superparamagnetism, i.e., the orientational thermal fluctuations of the particles' magnetic moments μ. Indeed, the measured temperature range is far from the Curie temperature of $CoFe_2O_4$, viz. 790 K; therefore, the reference thermal energy is far lower than the exchange energy so that the number of inverted spins in each particle is negligibly small and $\mu \simeq$ const at any temperature. On the other hand, at the same temperatures, the energy of relativistic interactions (magnetic anisotropy) that determines the direction of the particles' magnetic moment is quite comparable with thermal energy so that in the absence of an external field, the orientation of μ may easily diffuse.

The magnetic state of such a system is described by the distribution function W_{sys} of the directions of the magnetic moments of the constituent particles, and W_{sys}, in principle, parametrically depends on the material characteristics of each particle of the ensemble. Hereinafter, we treat all particles as spherical and as possessing the same magnetisation M_s and bulk anisotropy constant K but as different in (a) the particle radii and (b) the orientations of their magnetic anisotropy axes relative to the direction of the applied magnetic field.

The number of angular variables of the function W_{sys} is huge (twice the number of particles in the sample), which makes the study of its time evolution very difficult if one takes into account the interparticle interactions. For the case under study, however, strong simplifications may justifiably be applied. First, for particles with a mean diameter of 6 nm and a volume $V \sim 10^{-19}$ cm^3 at a volume concentration $\phi \sim 0.7$ vol.%, an estimate of the mean interparticle distance yields $\ell \sim (V/\phi)^{1/3} \sim 24$ nm, which by far excludes any significant contributions on the part of exchange-coupled particles.
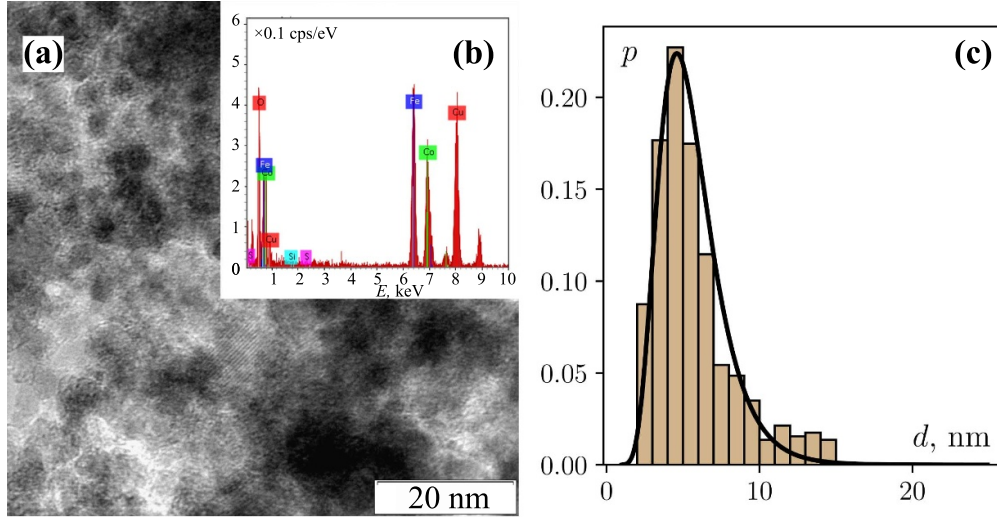
Figure 3. Size distribution histogram and typical HRTEM microphotograph of $CoFe_2O_4$ particles. The solid curve corresponds to an approximation by lognormal distribution with an average diameter of 5.6 nm and a root-mean-square deviation of 2.1 nm.
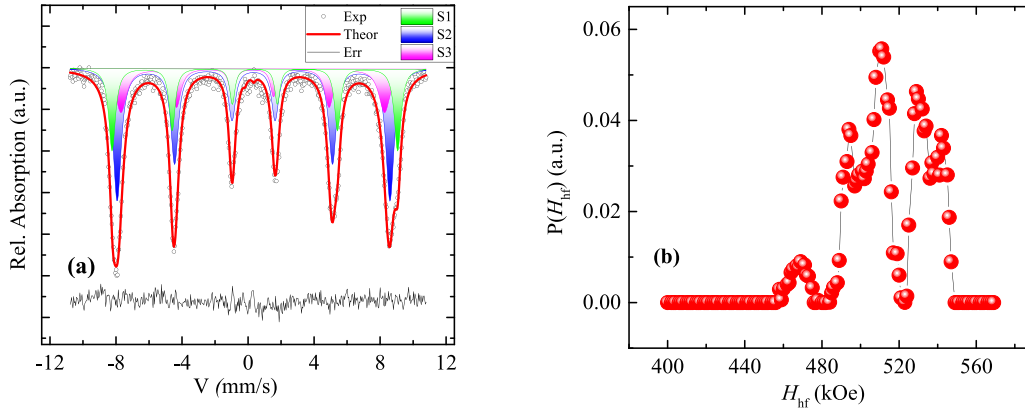

Figure 4. (a) Mössbauer spectrum of the investigated cobalt ferrite nanoparticle sample at $T = 4$ K; (b) the hyperfine field probability.

Table 1. Mössbauer spectral parameters. *IS* is the isomer shift relative to α-Fe, QS is quadrupole splitting, H_{rmhf} is the hyperfine field, *W* is the full width of the line at half-maximum, *dH* is the degree of nonuniformity of the hyperfine field, and *I* is the relative fraction in the spectrum.

IS, mm s^{-1} ± 0.005	H_{hf}, kOe g± 2	QS, mm s^{-1} ± 0.01	W, mm s^{-1} ± 0.01	dH, kOe ± 0.01	I, a.u. ± 0.03	Position
0.394	496	0.00	0.37	4	0.24	A
0.445	514	0.00	0.49	3	0.50	B
0.520	538	0.00	0.36	15	0.26	B

Second, the effect of interparticle magnetic dipole–dipole interactions might also be neglected. Indeed, the dipole–dipole energy per particle in the dispersion is $U_{dd} \sim \mu^2/\ell^3$; here, the magnetic moment of a single-domain particle is $\mu = M_s V$, and M_s is the saturation magnetisation of the ferrite. With these estimates for ℓ and μ, one obtains $U_{dd} \sim \phi M_s^2 V$. Even if to set $M_s \sim 450$ emu cm^{-3}, the same as that of bulk $CoFe_2O_4$, one gets $U_{dd} \sim 10^{-16}$ erg, i.e., about 2 K, which is well below the lowest temperature used in our measurements.

Given the above, the $CoFe_2O_4$ nanoparticles in the sample under study may be treated as statistically independent so that the full function W_{sys} splits into a product of the distribution

functions of individual particles, $W(\boldsymbol{e}, t)$, where $\boldsymbol{e} = \boldsymbol{\mu}/\mu$ is the unit vector of the direction of the particles' magnetic moment. The component of the ensemble magnetisation in the direction $\boldsymbol{h}$ of the applied field may then be written as

$$M = \boldsymbol{M} \cdot \boldsymbol{h} = M_0 \langle \boldsymbol{e} \cdot \boldsymbol{h} \rangle, \qquad (1)$$

where M_0 is the saturation magnetisation of the ensemble, and the angular brackets denote an average over the orientational distribution $W(\boldsymbol{e}, t)$, the particle size, and the tilt angles of the particles' anisotropy axes. The two latter distributions are obviously fixed in a sample by the end of synthesis and,
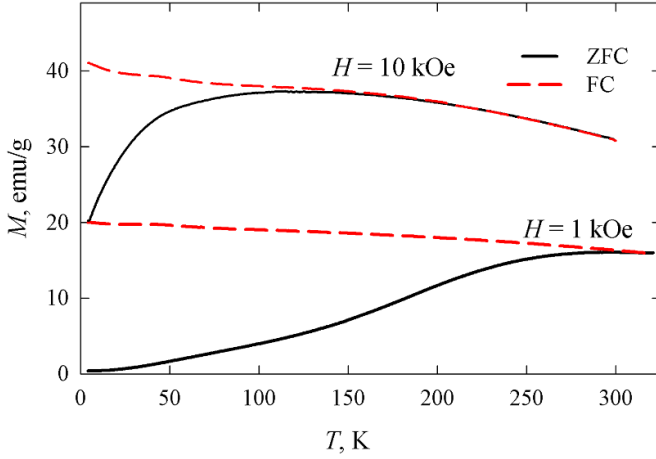
Figure 5. FC (dashes) and ZFC (solid lines) temperature dependences of magnetisation for the CoFe$_2$O$_4$ nanoparticles investigated, obtained under fields $H = 1$ and 10 kOe.

thus, do not depend on the magnetisation measurement protocol. On the other hand, the orientation distribution of the vector $\boldsymbol{\mu}$ of an individual particle, i.e., the function $W(\boldsymbol{e},t)$, strongly depends on the applied field $\boldsymbol{H}(t)$ and the rate of its variation.

The magnetic energy U of a single-domain particle comprises just two terms: the Zeeman energy in an external field and the contribution of magnetic anisotropy. We set the latter to be uniaxial since the spin–orbit interaction for the spins located on the surface has a reduced symmetry. This enables one to write U in the form

$$U = -\boldsymbol{\mu} \cdot \boldsymbol{H} - KV(\boldsymbol{e} \cdot \boldsymbol{n})^2, \tag{2}$$

where K is the bulk anisotropy constant, V is the particle volume, and $\boldsymbol{n}$ is the unit vector along the anisotropy axis; evidently, the standard Stoner-Wohlfarth model [58] is based on minimization of the energy function (2).

The time evolution of the orientational distribution function of the particles' magnetic moment is described by the Brown kinetic (Fokker-Planck-type) equation [59], which can be written in the operator form as

$$2\tau_D \frac{\partial W}{\partial t} = \hat{L}W, \tag{3}$$

where the reference time $\tau_D = (1+\alpha^2)\mu/2\alpha\gamma k_B T$, along with the value of the particles' magnetic moment μ, incorporate the Larmor precession damping parameter α, the gyromagnetic ratio γ, and the temperature T. The kinetic operator $\hat{L}$ on the right-hand side of (3) is defined as

$$\hat{L}W = \hat{\boldsymbol{J}} \cdot W \left(\hat{\boldsymbol{J}} + \frac{1}{\alpha} \frac{\partial}{\partial \boldsymbol{e}} \right) \left(\frac{U}{k_B T} + \ln W \right), \quad \hat{\boldsymbol{J}} = \boldsymbol{e} \times \frac{\partial}{\partial \boldsymbol{e}}.$$

Since equation (3) is linear with respect to function W, its solution can be expanded into a set of eigenfunctions of the operator $\hat{L}$ with time-dependent coefficients:

$$W(\boldsymbol{e},t) = F_0\big(\boldsymbol{e},\boldsymbol{H}(t)\big) + \sum_{i=1}^{\infty} A_i(t) F_i\big(\boldsymbol{e},\boldsymbol{H}(t)\big),$$

$$\hat{L}F_i\big(\boldsymbol{e},\boldsymbol{H}(t)\big) = -\lambda_i\big(\boldsymbol{H}(t)\big) F_i\big(\boldsymbol{e},\boldsymbol{H}(t)\big). \tag{4}$$

In this expression, the eigenmodes are arranged in the order of increase of the absolute values (magnitudes) of the real parts λ_i' of their eigenvalues. The eigenvalue λ_0 is zero and corresponds to a Boltzmann-like function $F_0 \propto \exp[-U(\boldsymbol{H}(t))/k_B T]$ which, however, parametrically depends on time.

The orientational relaxation of the magnetic moment of a uniaxial superparamagnetic particle in a DC field is well described in detail in [60–62]. The eigenvalue (decrement) λ_1 with the smallest absolute value (called the Néel one) is real and exponentially decreases with the growth of the magnetic anisotropy parameter $\sigma = KV/k_B T$ according to $\lambda_1 \sim (1/2\tau_D)e^{-\sigma}$. There is a significant qualitative difference between λ_1 and the decrements of all the rest modes, whose temperature dependence is much weaker: $\lambda_i' \sim i(i+1)/2\tau_D$ at $i > 1$.

The weight coefficients in expansion (4) have the following orders of magnitude: $A_i \sim \exp(-\lambda_i'\tau/2\tau_D)$, where τ is the reference timescale of the external field variation. If the frequency of the applied field is low ($\tau_D/\tau \ll 1$), then in the set of weight coefficients of expansion (4), function A_1, due to the exponential behaviour of λ_1, by far exceeds all the other functions: $A_1 \gg A_i$ ($i > 1$). As a result, in expansion (4), one may retain just the first mode.

For the cobalt ferrite particles under study, i.e., the ones with magnetisation $M \sim 80$ emu/g, the condition $\tau_D/\tau \ll 1$ undoubtedly holds for both field pulse lengths, $\tau = 8$ ms and 16 ms. For this reason, we hereinafter truncate the full expansion (4) to

$$W(\boldsymbol{e},t) = F_0\big(\boldsymbol{e},\boldsymbol{H}(t)\big) + A_1(t) F_1\big(\boldsymbol{e},\boldsymbol{H}(t)\big). \tag{5}$$

A reliable approximate expression for the function F_1 was derived in [63]:

$$F_1(\boldsymbol{e},\boldsymbol{H}(t)) = \begin{cases} e^{-U(\boldsymbol{e},\boldsymbol{H}(t))/T}/Z_1\big(\boldsymbol{H}(t)\big), & \text{for} \quad \boldsymbol{e} \in \Omega_1; \\ -e^{-U(\boldsymbol{e},\boldsymbol{H}(t))/T}/Z_2\big(\boldsymbol{H}(t)\big), & \text{for} \quad \boldsymbol{e} \in \Omega_2. \end{cases} \tag{6}$$

In this formula, the partial statistical integrals Z_1 and Z_2 are calculated within the intervals $\Omega_1 = \{0 \leqslant \vartheta < \vartheta_s, 0 \leqslant \varphi \leqslant 2\pi\}$, and $\Omega_2 = \{\vartheta_s \leqslant \vartheta < \pi, 0 \leqslant \varphi \leqslant 2\pi\}$, respectively. The angles are specified in a spherical coordinate framework, with the polar axis directed along the anisotropy axis of the particle; the angle ϑ_s is the polar coordinate of the saddle point of the potential energy (2).

Substituting equation (5) into kinetic equation (3) with allowance for (6), we reduce the problem to the ordinary differential equation for the unknown coefficient $A_1(t)$:

$$\frac{dA_1(t)}{dt} + \frac{\lambda_1(t)}{2\tau_D} A_1(t) = -\frac{1}{2}\frac{d}{dt}\left(\frac{Z_1 - Z_2}{Z_1 + Z_2} \right). \tag{7}$$

Solving numerically this equation, one can find $A_1(t)$ and then, using formula (5), recover function $W(\boldsymbol{e},t)$.
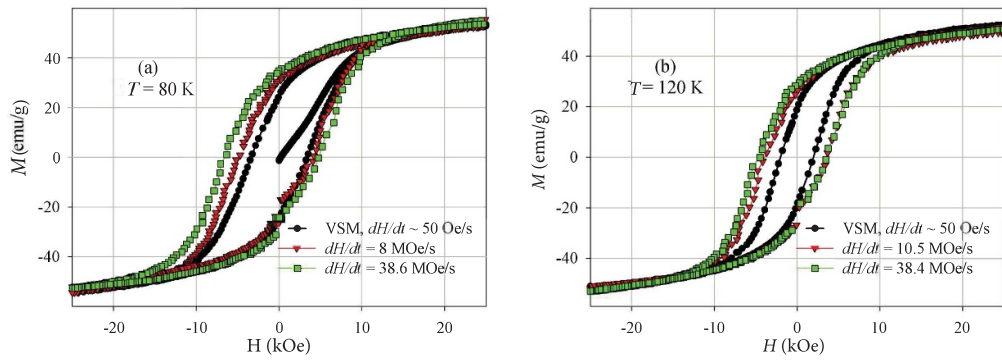
Figure 6. Hysteresis loops obtained by the VSM technique and in pulse fields at different external field variation rates *dH/dt* at temperatures: (a) 80 K and (b) 120 K.

Table 2. Parameters of the hysteresis loops of figure 6.

Figure	dH/dt, MOe s^{-1}	τ_P, ms	H_0, kOe
6(a)	8	16	51
6(a)	38.6	8	110
6(b)	10.55	16	66
6(b)	38.4	8	111

To interpret the magnetisation curves shown in figure 6, we assume that during the time lapse equal to the pulse length τ, the applied field evolves according to $H(t) = H_0 \cos 2\pi t/\tau$; a tiny deviation of the real signal profile from a perfect sinusoid is confirmed by figure 1. The magnetisation component directed along the field, i.e. the component that is registered in the experiment is calculated for each instant of time using equation (1), where averaging is performed over (a) the orientation of the magnetic moment of an individual particle with the aid of the distribution function $W(e, t)$, (b) the orientation of the easily magnetised axes of the particles comprising the ensemble is assumed to be random, and (c) the particle size, whose distribution is rendered by the lognormal function shown in figure 3. The $M(H)$ curve is obtained by eliminating time from the pair of evolution functions $M(t)$ and $H(t)$, and the coercivity H_c is determined from the condition $M(H_c) = 0$.

5. Discussion

Figure 7 provides a comparison of the coercivity values measured and numerically calculated at different temperatures. It can be seen that the model calculation yields fairly good agreement between the theoretical curve and the experimental points; the value of the anisotropy constant used is $K = 6.0 \times 10^6$ erg cm^{-3}.

The temperature-independent anisotropy constant $K \simeq 6.0 \times 10^6$ erg cm^{-3} obtained by fitting the theory to our experiment should be compared to the K_{eff} values reported in other works on the subject. Upon attempting this, one finds that the published data on the K_{eff} of nanodisperse CoFe$_2$O$_4$ are rather diverse. In particular, according to the measurements of references [16, 19, 31–34] the values of K_{eff} at low temperatures are in the range of

$(2.5–4) \times 10^6$ erg cm^{-3}. On the other hand, in many works [1, 26, 28, 40–42] much higher experimental estimates were made for K_{eff}: $(7–10) \times 10^6$ erg cm^{-3} and, in a single case, even 37×10^6 erg cm^{-3} [22]. For completeness, we also refer to two communications where the measured values of K_{eff} are extremely low: $\sim 1.5 \times 10^6$ erg cm^{-3} [23, 29]. Finally, note that the anisotropy constant for bulk CoFe$_2$O$_4$ crystals is $(1.8–3) \times 10^6$ erg cm^{-3}.

A specific feature of the nano-CoFe$_2$O$_4$ samples which display high anisotropy is the chemical synthesis of particles involving organic compounds. In particular, in [40] a necessary component in the synthesis of particles $3.5 \div 6.3$ nm in size was oleic acid, which strongly affected the magnetic properties of the sample. Thus, the value of K obtained for our particles is expected to be of the same order of magnitude since they were also synthesized in the presence of organic molecules.

A worthwhile insight into this issue was published recently in [64], which explored solid dispersions of nano-CoFe$_2$O$_4$ with a mean particle diameter $d = 6.85$ nm both experimentally and theoretically. The leading idea is that since CoFe$_2$O$_4$ is a complex inverse spinel, different methods of synthesis yield particles with the same elemental content but with different proportions between the Fe and Co cations occupying the A and B elementary cell sites, respectively; this proportion is characterized by the index x in the formula $(Co_{1-x}Fe_x)(Co_xFe_{2-x})O_4$. With the aid of first-principles calculations, whose results were then fed to a micromagnetic simulator, MuMax3, the authors showed that variation of the inversion index x entails substantial changes in the width of the magnetisation loops (i.e. the coercivity) of CoFe$_2$O$_4$ nanoparticles. By comparing the model loops obtained with VSM measurements of their samples, the authors of [64] found a very reasonable estimate for the numerical range of inversion index x of the ferrite their particles consisted of. We note that the particles investigated in [64] were very similar in size to those studied in our work. Moreover, the inversion indices x of both species turn out to be quite close in the sense that according to calculations by Freire *et al*, the coercive forces for nano-CoFe$_2$O$_4$ with $x = 0.75$ (as in [64]) and $x = 0.5$ (our work) are very close. Therefore, it does not seem a coincidence that the estimate for the anisotropy constant (5.85×10^6 erg

Figure 8. Temperature dependence of the dynamic coercivity in the quasi static mode (VSM) at the field variation rate of $dH/dt = 20$ MOe s^{-1}; symbols correspond to measurements, and lines to calculations according to the superparamagnetic model. The precession damping parameter is $\alpha = 0.1$, and the anisotropy constant is $K = 6.0 \times 10^6$ erg cm^{-3}.
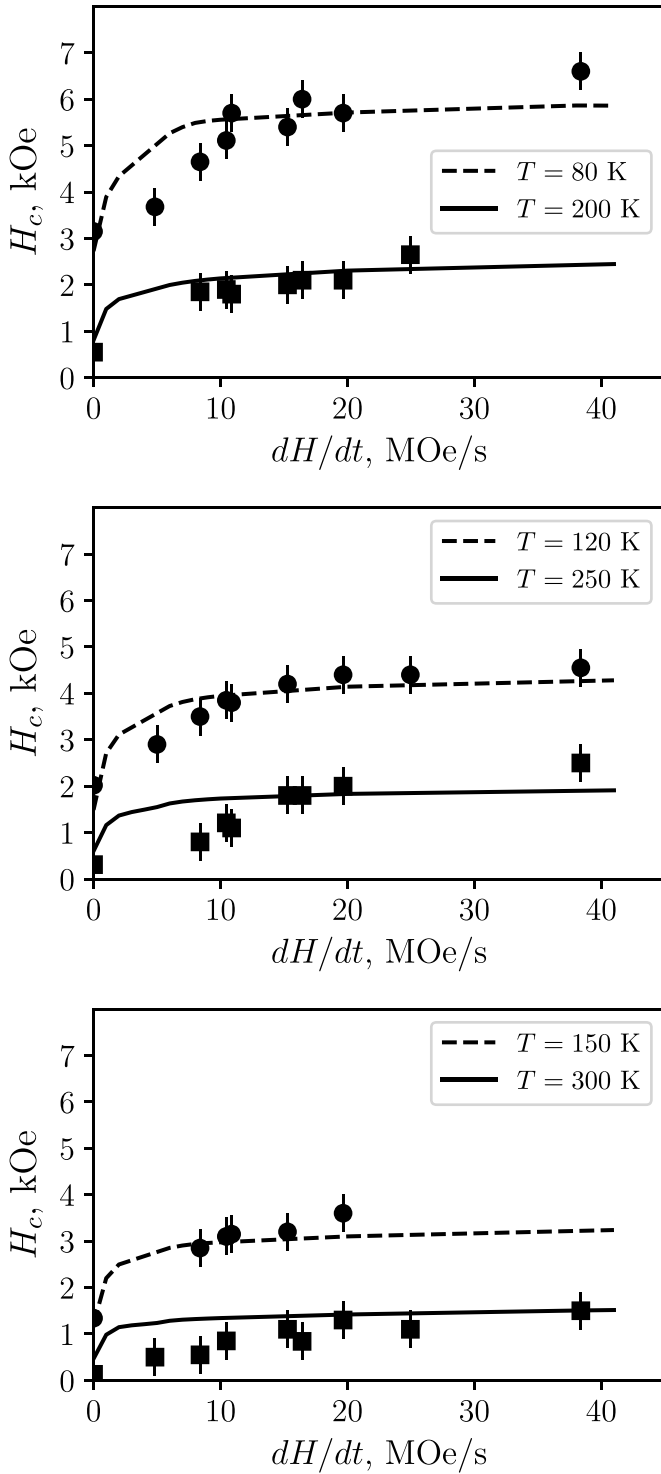
Figure 7. Dependence of dynamic coercivity on the field variation rate dH/dt at different temperatures; dots correspond to the measurements, and lines to the superparamagnetic theory; the precession damping parameter is $\alpha = 0.1$ and the anisotropy constant is $K = 6.0 \times 10^6$ erg cm^{-3}.

cm^{-3}) given in [64] is in excellent agreement with the value ($K = 6.0 \times 10^6$ erg cm^{-3}) that resulted from our fitting.

For further discussion, it is instructive to present our theoretical vs. experimental comparison in a customary form, i.e., as the temperature dependence of the coercivity H_c
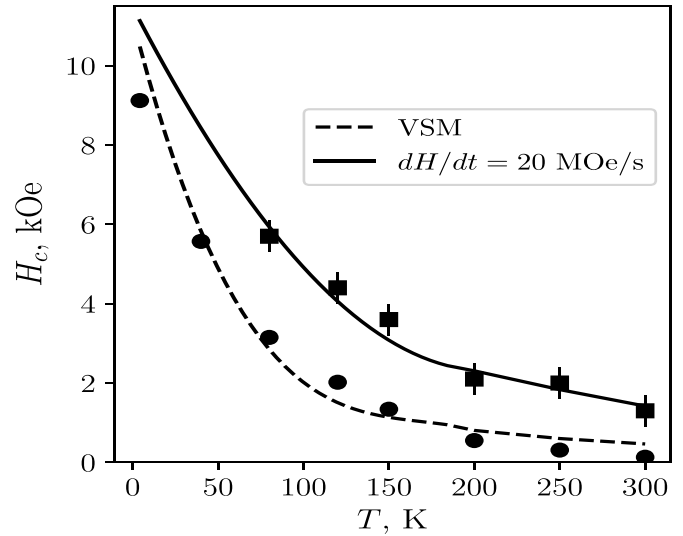
under constant dH/dt values. Figure 8, shows the functions $H_c(T)$ in the quasi static limit and at a field variation rate of $dH/dt = 20$ MOe s^{-1}. As can be seen, the sequences of experimental points evidence virtual 'thawing' of the coercivity that might be attributed to a decrease in the intrinsic material parameter K_{eff} of the particles. This viewpoint currently prevails in the literature, see the above-cited works [1, 15, 16, 18, 19, 22, 23, 25, 26, 29, 34, 37].

The superparamagnetic concept, as such, is not completely excluded from consideration, however. It is frequently used in its simplest form by assuming that below a blocking temperature T_B, the particles are fully ferromagnetic, whereas above T_B they are virtually paramagnetic with zero coercivity [18, 20, 24, 27, 34, 40]. This approach was extended in [37], where the authors made use of the Néel-Brown formula for the relaxation time [59] for the case of a small applied field and introduced a distribution function for the blocking temperatures. In this model, the temperature dependence of coercivity has the form $H_c(T) \propto \left[1 - (T/\langle T_B \rangle_T)^{1/2}\right]$, where the distribution function used to average the blocking temperature over the interval $[\infty, T]$ is defined as $f(T_B) \propto d[M_{\text{ZFC}} - M_{\text{FC}}]/dT$ and is to be measured experimentally over a wide temperature range. Indeed, the authors of [37] indeed obtained a fairly good agreement with their measurements of coercivity. However, their model resembles a useful recipe for deriving the $H_c(T)$ dependence from a large amount of experimental data on ZFC and FC magnetisations (which have to be measured anew for each sample), rather than a theory with any predictive force.

The model, in the framework of which we obtained the theoretical curves of figure 8, is essentially different. These plots were obtained on a unified basis, see section 4, under the assumption that the anisotropy constant

$K = 6.0 \times 10^6$ erg cm^{-3} depends neither on temperature nor on the particle size. The only cause of the temperature drop ('thawing') of the anisotropy presented in figure 8 is the thermal fluctuational (superparamagnetic) effect that is consistently taken into account; it is all the more clear since the parameter K is kept constant. Note also that in our model, the averaging is taken over a directly measurable quantity, the particle size, that is evaluated independently of any magnetic measurements.

Therefore, the results presented above establish that a significant decrease in coercivity H_c upon heating the system encountered in our and many other experiments is mainly due to thermal perturbations of the directions of the magnetic moment of single-domain particles. In other words, our theory shows that the observed change in coercivity is a manifestation of the universal thermal fluctuational effect and, as such, should, to a certain extent, be inherent to all magnetic nanosystems.

We would like to emphasize that the entire insensitivity of the anisotropy constant to thermal fluctuations and the independence of K from the particle size, is a model assumption. In reality, the parameter K most probably has its own temperature dependence that stems from the microstructure of a particular ferrite—the inversion degree of the ferrite, the presence of defects, etc—and because of that, it is highly likely to change with the particle size. For instance, such modifications may be responsible for some deviations between theory and experiment within the studied temperature interval, see figure 8. However, based on the overall behavior of the data points and theoretical plots, it follows that the intrinsic temperature dependence of the anisotropy parameter, although able to a certain extent to modify the results of our simple superparamagnetic theory, does not touch upon the general trend that the latter reveals quite clearly.

Finally, let us address the issue of distinguishing pure bulk anisotropy from the combined bulk and surface anisotropy of the particles. As mentioned, without a well-verified experimental size dependence of the coercive field, it is impossible to make any positive conclusions. However, our results allow one to estimate the upper bound for the surface anisotropy constant of our particles assuming the combined case:

$$K = K_v + 6K_s/\overline{d}, \tag{8}$$

where K_v and K_s are the bulk and surface anisotropy constants, respectively. Setting the mean particle diameter $\overline{d} \approx 6$ nm and $K_v \simeq 2 \times 10^6$ erg cm^{-3}, which is the reference value for massive CoFe$_2$O$_4$ crystals, using equation (8), one gets $K_s \simeq 0.4$ erg cm^{-2}.

Indeed, the estimation of K_s derived by splitting the anisotropy constant obtained from a solution that initially just has a bulk K might seem incorrect. Although formally so, the possible discrepancies are minimal. Indeed, in the framework of our model, the difference in the size dependence of the components of K is only important for the final stage of averaging: that with respect to the particle diameter. To check the difference in the effects of the results for equal values of K (bulk) and $K = K_v + 6K_s/\overline{d}$, we performed several test calculations

(K_s was varied); however, their results turned out to differ from the presented ones by just 1%–2% and because of that, they are not shown.

The upper bound obtained for K_s is quite a high value if we compare it with the respective estimates for the maghemite particles of about the same diameter, where $K_s \sim 0.03$ erg cm^{-2} [45]. However, we note that given the low value of the bulk anisotropy of maghemite itself and the fact that the value of K_s given above is the maximum value for nano-CoFe$_2$O$_4$, such a comparison could hardly be very informative. It is much more instructive to compare our results to the recently published experimental estimates for nano-CoFe$_2$O$_4$ [44]. For particles with $d \leqslant 16$ nm, the authors reported a value of $\tilde{K}_s \simeq 7.4 \times 10^6$ erg cm^{-3} (note that this is expressed in volume density units). Transformation according to equation (8) gives $K_s = \tilde{K}_s\overline{d}/6$, from which, upon setting $\overline{d} = 16$ nm, one gets the value $Ks \sim 2.0$ erg cm^{-2} for the nanoparticles of [44] , i.e., about four times greater than what we have. However, if we set $\overline{d} = 6$ nm, as in our samples, then the same estimate yields $K_s \sim 0.75$ erg cm^{-2}, which is reasonably close to our result.

6. Conclusions

In laboratory practice, nanodisperse cobalt ferrites have been synthesized by different physicochemical methods. It turns out that the particular synthesis technique significantly affects the magnetic characteristics of particles, including their magnetic anisotropies, both bulk and surface. The fundamental characteristics of the latter are the symmetry type and the values of the corresponding parameters K_{eff} or K_v and K_s. Under the assumption of uniaxial symmetry of the nanoparticles' anisotropy, we show that, at any specified temperature-independent value of the anisotropy constant (bulk or combined), the temperature dependence of the measured coercivity H_c of a particle or an assembly of those is, in the first place, determined by the thermal fluctuational (superparamagnetic) effect and, as such, is universal. The proposed theoretical model, which explicitly takes into account the kinetic effects not only explains the experimentally observed 'thawing' of the anisotropy of nano-CoFe$_2$O$_4$ but also allows us to predict the dependence of the dynamic coercivity H_c on the frequency of the applied field.

Data availability statement

The data that support the findings of this study are available upon reasonable request from the authors.

Acknowledgments

J. Phys. D: Appl. Phys. **54** (2021) 275003

D A Balaev *et al*

ORCID iDs

A A Krasikov ⑩ https://orcid.org/0000-0002-0756-0495
Yu L Raikher ⑩ https://orcid.org/0000-0002-6167-6528

References

[1] López-Ortega A, Lottini E, de Julián Fernández C and Sangregorio C 2015 *Chem. Mater.* **27** 4048–56
[2] Pedrosa F J, Rial J, Golasinski K M, Guzik M N, Quesada A, Fernández J F, Deledda S, Camarero J and Bollero A 2016 *Appl. Phys. Lett.* **109** 223105
[3] Pal M, Kundu A, Rakshit R and Mandal K 2015 *ChemPhysChem* **16** 1627–34
[4] Kazemi M, Ghobadi M and Mirzaie A 2017 *Nanotechnol. Rev.* **7** 43–68
[5] Loan N T T, Lan N T H, Hang N T T, Hai N Q, Anh D T T, Hau V T, Tan L V and Tran T V 2019 *Processes* **7** 885
[6] Vamvakidis K, Kostitsi T M, Makridis A and Dendrinou-Samara C 2020 *Materials* **13** 1537
[7] Hassan M R and Aly M I 2020 *Particulate Sci. Technol.* **38** 236–46
[8] Srinivasan S Y, Paknikar K M, Bodas D and Gajbhiye V 2018 *Nanomedicine* **13** 1221–38
[9] Wang T, Jiang Z, An T, Li G, Zhao H and Wong P K 2018 *Environ. Sci. Technol.* **52** 4774–84
[10] Baldi G, Bonacchi D, Franchini M C, Gentili D, Lorenzi G, Ricci A and Ravagli C 2007 *Langmuir* **23** 4026–8
[11] Amiri S and Shokrollahi H 2013 *Mater. Sci. Eng.* C **33** 1–8
[12] Yadavalli T, Jain H, Chandrasekharan G and Chennakesavulu R 2016 *AIP Adv.* **6** 055904
[13] Ashour A H, El-Batal A I, Maksoud M I A A, El-Sayyad G S, Labib S, Abdeltwab E and El-Okr M M 2018 *Particuology* **40** 141–51
[14] Moumen N and Pileni M P 1996 *Chem. Mater.* **8** 1128–34
[15] Chinnasamy C N, Jeyadevan B, Shinoda K, Tohji K, Djayaprawira D J, Takahashi M, Joseyphus R J and Narayanasamy A 2003 *Appl. Phys. Lett.* **83** 2862–4
[16] Tung L D, Kolesnichenko V, Caruntu D, Chou N H, O'Connor C J and Spinu L 2003 *J. Appl. Phys.* **93** 7486–8
[17] Hutlova A, Niznansky D, Rehspringer J L, Estournès C and Kurmoo M 2003 *Adv. Mater.* **15** 622–5
[18] Vejpravová J, Sechovský V, Plocek J, Nižňanský D, Hutlová A and Rehspringer J L 2005 *J. Appl. Phys.* **97** 124304
[19] Virden A, Wells S and O'Grady K 2007 *J. Magn. Magn. Mater.* **316** e768–71
[20] Peddis D, Cannas C, Musinu A and Piccaluga G 2008 *J. Phys. Chem.* B **112** 8507–13
[21] Peddis D, Mansilla M V, Mørup S, Cannas C, Musinu A, Piccaluga G, D'Orazio F, Lucari F and Fiorani D 2008 *J. Phys. Chem.* B **112** 5141–7
[22] Toksha B G, Shirsath S E, Patange S M and Jadhav K M 2008 *Solid State Commun.* **147** 479–83
[23] Desautels R D, Cadogan J M and van Lierop J 2009 *J. Appl. Phys.* **105** 07b506
[24] Cannas C *et al* 2010 *Chem. Mater.* **22** 3353–61
[25] Peddis D, Cannas C, Musinu A, Piccaluga G, Agostinelli E and Fiorani D 2010 *Nanotechnology* **21** 125705
[26] Vázquez-Vázquez C, López-Quintela M A, Buján-Núñez M C and Rivas J 2011 *J. Nanopart. Res.* **13** 1663–76
[27] Artus M, Ben Tahar L, Herbst F, Smiri L, Villain F, Yaacoub N and Grenèche J-M 2011 *J. Phys.: Condens. Matter* **23** 506001
[28] Peddis D, Orrù F, Ardu A, Cannas C, Musinu A and Piccaluga G 2012 *Chem. Mater.* **24** 1062–71
[29] Topkaya R, Akman Õ, Kazan S, Aktas B, Durmus Z and Bayka A 2012 *J. Nanopart. Res.* **14** 1156
[30] Hannour A, Vincent D, Kahlouche F, Tchangoulian A, Neveu S and Dupuis V 2014 *J. Magn. Magn. Mater.* **353** 29–33
[31] Mohapatra J, Mitra A, Bahadur D and Aslam M 2015 *J. Alloys Compd.* **628** 416–23
[32] Pianciola B N, Lima E, Troiani H E, Nagamine L C C M, Cohen R and Zysler R D 2015 *J. Magn. Magn. Mater.* **377** 44–51
[33] Xu S T, Ma Y Q, Xu Y F, Sun X, Geng B Q, Zheng G H and Dai Z X 2015 *Mater. Res. Bull.* **62** 142–7
[34] Xu S T, Ma Y Q, Zheng G H and Dai Z X 2015 *Nanoscale* **7** 6520–6
[35] Lu L T, Dung N T, Tung L D, Thanh C T, Quy O K, Chuc N V, Maenosono S and Thanh N T K 2015 *Nanoscale* **7** 19596–19610
[36] Lima A C, Morales M A, Araújo J H, Soares J M, Melo D M A and Carriço A S 2015 *Ceram. Int.* **41** 11804–9
[37] Carvalho M H, Lima R J S, Meneses C T, Folly W S D, Sarmento V H V, Coelho V H V and Duque J G S 2016 *J. Appl. Phys.* **119** 093909
[38] Batoo K M, Salah D, Kumar G, Kumar A, Singh M, El-sadek M A, Mir F A, Imran A and Jameel D A 2016 *J. Magn. Magn. Mater.* **411** 91–7
[39] Rani B J, Ravina M, Saravanakumar B, Ravi G, Ganesh V, Ravichandran S and Yuvakkumar R 2018 *Nano-Syst. Nano-Objects* **14** 84–91
[40] Ansari S M, Sinha B B, Phase D, Sen D, Sastry P U, Kolekar Y D and Ramana C V 2019 *ACS Appl. Nanomater.* **2** 1828–43
[41] Aslibeiki B, Kameli P, Salamati H, Concas G, Fernandez M S, Talone A, Muscas G and Peddis D 2019 *Beilstein J. Nanotechnol.* **10** 856–65
[42] Muscas G *et al* 2019 *IEEE Magn. Lett.* **10** 6110305
[43] Moreira A F L, Paula F L O, Campos A F C and Depeyrot J 2020 *J. Solid State Chem.* **286** 121269
[44] Mohapatra J, Xing M, Elkins J, Beatty J and Liu J P 2020 *J. Phys. D: Appl. Phys.* **53** 504004
[45] Shilov V P, Bacri J-C, Gazeau F, Gendrone F, Perzynski R and Raikher Y L 1999 *J. Appl. Phys.* **85** 6642–7
[46] Lavorato G *et al* 2016 *Phys. Rev.* B **94** 054432
[47] Hasz K, Ijiri Y, Krycka K L, Borchers J A, Booth R A, Oberdick S and Majetich S A 2014 *Phys. Rev.* B **90** 180405
[48] Peddis D *et al* 1999 *J. Phys.: Condens. Matter.* **23** 426004
[49] Zákutná D, Niznanský D, Barnsley L C, Babcock E, Salhi Z, Feoktystov A, Honecker D and Disch S 2020 *Phys. Rev.* X **10** 031019
[50] Kirillov V L *et al* 2019 *Mater. Chem. Phys.* **225** 292–7
[51] Balaev A D, Boyarshinov Y V, Karpenko M M and Khrustalev B P 1985 *Instrum. Exp. Tech. (English translation)* **26** 167–8 (https://www.osti.gov/biblio/5496232)
[52] Grigorova M *et al* 1998 *J. Magn. Magn. Mater.* **183** 163–72
[53] Kim S J, Lee S W and Kim C S 2001 *Japan. J. Appl. Phys.* **40** 4897–902
[54] Haneda K and Morrish A H 1988 *J. Appl. Phys.* **63** 4258–60
[55] Baldi G, Bonacchi D, Innocenti C, Lorenzi G and Sangregorio C 2007 *J. Magn. Magn. Mater.* **311** 10–16
[56] Vargas J M, Srivastava A, Yourdkhani A, Zaldivar L, Caruntu G and Spinu L 2011 *J. Appl. Phys.* **110** 064304
[57] Peddis D, Cannas C, Musinu A and Piccaluga G 2009 *Chem. Eur.* J. **15** 7822–9
[58] Stoner E C and Wohlfarth E P 1948 *Phil. Trans. R. Soc.* A **240** 599–642
[59] Brown W F 1963 *Phys. Rev.* **130** 1677–86

J. Phys. D: Appl. Phys. **54** (2021) 275003

D A Balaev *et al*

[60] Coffey W T, Crothers D S F, Dormann J L, Geoghegan L J,
     Kalmykov Y P, Waldron J T and Wickstead A W 1995
     Phys. Rev. B **52** 15951–6
[61] Raikher Y L and Stepanov V I 2002 *Phys. Rev.* B **66** 214406

[62] Kalmykov Y P 2004 *J. Appl. Phys.* **96** 1138–45
[63] Poperechny I S and Raikher Y L 2014 *Phys.* B **435** 58–61
[64] Freire R M, Palma J L, Michea S, Ramirez R, Baltazar S E and
     Denardin J C 2021 *Inorg. Chem. Frontiers* **8** 433–43